Unsteadiness in supersonic Free Shock Separation in overexpanded flows

Naima Demni, Sébastien Piponniau, Pierre Dupont

Unsteadiness in supersonic Free Shock Separation in overexpanded flows

Naima Demni *, Sébastien Piponniau†, Julien Herpe ‡, Pierre Dupont§

While operating in an overexpanded condition, nozzles exhibit side loads. These loads are due to the presence of unsteadiness in the shock wave boundary layer interactions which are developing inside the nozzle. This paper deals with an interaction, which compares with Free Shock Separation regime, and occurs when the boundary layer doesn't reattach to the floor. We present the first results on an original experimental set-up of a 2D Free Shock Separation, at Mach number of 2.1. Pitot probe, static pressure probe, hot wire anemometry and Particle Image Velocimetry are used to describe the spatial organization of the flow, as well as the frequency scales obtained in various configurations. No evidence of intrinsic low time scales of the shock has been observed and the dominant frequencies of the shock spectrum are found similar to that of the subsonic external flow. Nevertheless, the amplitude of the low frequency motions are found to increase when the flow separates.

I. Nomenclature

P_2	=	Static pressure at the outlet of the injection system
P_1	=	Static pressure of the outlet of the wind tunnel at M=2.1
P_1'	=	Static pressure after the expansion
$\frac{P_2}{P_1'}$	=	pressure ratio through the separation shock wave
θ	=	Expansion angle
φ	=	Streamlines deflection
β	=	Shock wave angle
$\dot{m}$	=	Injected mass flux
FSS	=	Free Shock Separation
RSS	=	Restricted Shock Separation
$SWBLI$	=	Shock Wave Boundary Layer Interaction
M_1'	=	incoming Mach number, downstream the expansion
Cf	=	incoming friction coefficient, downstream the expansion
u_τ	=	incoming friction velocity, downstream the expansion
δ	=	incoming boundary layer thickness, downstream the expansion
δ_*	=	incoming boundary layer displacement thickness, downstream the expansion
L_{exp}	=	Shock wave excursion length
L	=	Shock wave interaction length corresponding to the distance of the shock foot from the lip
μ	=	dynamic viscosity
F_{fit}	=	universal Shapman function
q_0	=	incoming dynamic pressure, downstream the expansion
$P(\bar{x_0})$	=	pressure in the separation point
$P(\bar{x})$	=	pressure in the separation zone
e	=	Constant ($log(e) = 1$)

*PhD, Centre National d'Études Spatiales CNES, DLA; Aix-Marseille Université, France.
†Associate professor, IUSTI UMR Aix-Marseille Université - CNRS 7343, France
‡Centre National d'Études Spatiales
§Senior scientist, IUSTI, UMR Aix-Marseille Université - CNRS 7343, France

II. Introduction

During a rocket's engine start-up, as well as in the flight's low altitudes, the pressure inside the nozzle is much lower than the external ambient pressure. This leads to an adverse pressure gradient that induces a streamlines deviation from the wall, a flow separation, and a creation of a shock wave. This shock wave is unsteady and leads to important aerodynamic and thermal loads on the nozzle's structure.

The shock unsteadiness is characterized by low frequencies. The study of the origins of theses frequencies was quite investigated in a particular separation configuration: Restricted Shock Separation, which occurs when the flow gets detached from the wall and reattach downstream. In this case, different mechanisms were suggested to explain the dilatation and contraction of the recirculation bubble and the correlation between this "breathing" movement and the shock's fluctuations. In [1], the contraction/expansion of the recirculation bubble was associated to the extraction of a mass flux from the bubble to contribute to the thickening of the mixing layer. It was found out that this mass extraction occurs at a frequency (or Strouhal number) close to that of the shock. Other suggestions have been proposed in the literature to relate the low frequencies shock motions to an equivalent low pass filter applied by the interaction to the upstream perturbations ([2–6]). These upstream perturbations can involve very large length scales, up to scales almost $30 * \delta_{99}$, and have been found to modulate the shock unsteadiness in high Reynolds number interactions [7]. In addition, low frequency unsteadiness has been associated with the development of Görtler-like structures along the interaction [8].

The present study deals with the shock unsteadiness in an other configuration, which is the Free Shock Separation. In this case, the separated shear layer doesn't reattach downstream. A new set up has been developed in order to generate such a flow in a 2D configuration. The idea is to generate a shock separation downstream a boundary layer expansion, as can be found in an over-expanded nozzle. First, we tend to set up the expansion, then, we impose an adverse pressure gradient through an over-pressured low speed secondary flow which promotes the flow separation and allows mass injection inside the interaction. We might expect that the mean fields in the initial part of the separation region will exhibit similar properties as observed in restricted separations [9], but they will differ dramatically when the downstream region is considered. Therefore, it is suitable to validate the generality of the different models proposed to explain the origin of the low frequency unsteadiness in shock induced separations.

The 2D configuration allows to use classical anemometry to document the mean and unsteady fields. Thanks to unsteady pressure, hot wire measurements and Particle Image Velocimetry, we will be able to measure the characteristic length and time scales of the incoming boundary layer and the separation. They will be compared with classical results obtained in 2D Shock Wave Boundary Layer Interactions.

III. Experimental setup used to generate the Free Shock Separation

This experimental work was carried out in the hypo-turbulent supersonic wind tunnel of the IUSTI laboratory in Marseille, France. It's a continuous operating wind tunnel. The outlet Mach number of the test section is 2.1 and the stagnation pressure is set to 0.6 atm. It is a closed-loop circuit and the stagnation conditions are maintained nearly constant: the variation of the stagnation temperature is less than 1 degree per hour..

The objective is to create a bi-dimensional experimental configuration of a free shock separation. Thus, we don't take into account the tridimensional or axisymmetric effects existing in a nozzle. The shock separation in an over-expanded nozzle is due to the gap between the low pressure inside the nozzle and the external atmospheric pressure. In order to simulate accurately this phenomenon, we impose an expansion wave in the supersonic flow that play the role of the nozzle's divergent shape that lowers the pressure. Therefore, the static pressure of the incoming expanded boundary layer decreases from P_1 to P'_1 which depends on the amount of the expansion. In addition, we inject a mass flux at the test section's outlet, at a static pressure $P_2 > P'_1$, which plays the role of the atmospheric pressure. The ratio $\frac{P_2}{P'_1}$ determines the intensity of the shock wave separation. The experimental principle is presented on Figure 1.

The expansion is generated by a sharped leading edge fixed accross the lateral windows of the test section, with a variable inclination angle θ, presented on figure 2. The injected mass flux $\dot{m}$ is generated by a system based on a nozzle with a sonic throat. Thus, we can change the mass flux by varying the throat's section or/and the total pressure upstream. By varying $\dot{m}$ (consequently P_2), and θ (consequently P'_1), we vary the intensity of the separation through the ratio $\frac{P_2}{P'_1}$. With this system, ratios $\frac{P_2}{P'_1}$ from 1.5 to 2.1 have been obtained. The maximal pressure ratio $\frac{P_2}{P'_1} = 2.1$ corresponds to $\dot{m} = \dot{m}_1$, θ=6.5 °. This case will be detailed in this work: it will be shown that it corresponds to a separated interaction. We note that the shock wave is located in an isobar zone downstream from the expansion, so that the upstream static pressure before the separation shock wave is P'_1 (see figure 1). In an over-expanded nozzle, the shock location is governed by a pressure condition. In this new configuration, the shock location is not fixed by such condition and should

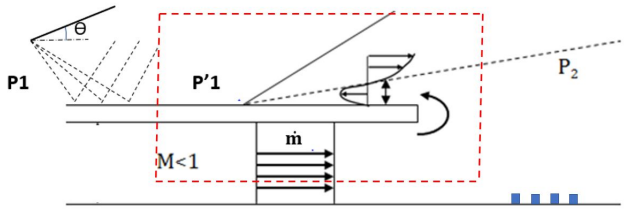

Fig. 1 Illustrative scheme of the 2D FSS configuration. The red dashed lines indicate the PIV FOV, the blue squares indicate the Kulites probes at the wall

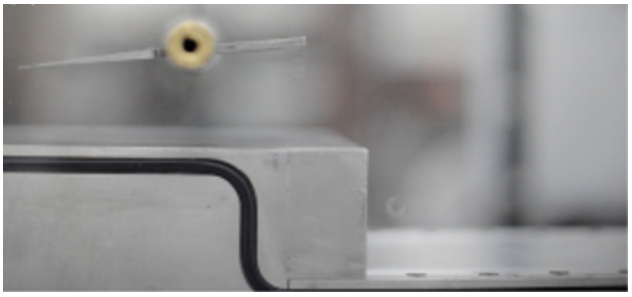

Fig. 2 Fin used to generate the expansion waves, fixed in the ceiling of the wind tunnel.

follow classical laws established in Shock Wave Boundary Layer Interactions [10]. Therefore, this is an intermediate configuration between classical SWBLI but without reattachment downstream the separation, and a FSS configuration where the shock location is defined by pressure equilibrium. It will allow to separate the effect of the pressure gradient associated with the expansion generated by the nozzle.

For the mean description of the flow, longitudinal static pressure measurements are acquired along the expansion and through the interaction region. Furthermore, two components PIV is performed with a field of view as indicated Figure 1 with a high space resolution. A Dantec Dynamics two components system is used. The main parameters of the PIV system are:

- 11 MP high sense camera
- 200 mJ laser
- 51 pixels/mm resolution to assure accurate turbulent measurements
- 1µs delay time between frames

Incense smoke has been used to seed the flow and statistics are derived from 2000 snapshots. The seeding was similar to the one used in previous SWBLI studies [1]. The light sheets are generated using an endoscope placed in the diffuser of the test section, with a 1200mm lens. Concerning the temporal properties of the interaction, shock and downstream subsonic flow unsteadiness are documented with hot wire anemometry and unsteady wall pressure transducers (Kulite probes) . A Streamline Dantec CTA anemometer has been used in symmetric bridge configuration with 5µm wires. The typical bandwidth for our aerodynamic configuration is about 100kHz. Four Kulites are flushed mounted inside the floor of the test section downstream the trailing edge of the plate separating the supersonic and subsonic flow. Their location is reported Figure1. A fifth Kulite is installed upstream in the injection system in order to identify any acoustic resonance in the pipes of injection. A high speed digital converter with 14bits resolution is used to acquire simultaneously the hot wire and Kulite signals at a sampling frequency of 200kHz for a duration of 10sec.

IV. Mean organization of the interaction

The mean fields properties of the case $\dot{m} = \dot{m}_1$, θ=6.5 °, which corresponds to a pressure ratio $\frac{P_2}{P_1'} = 2.1$ are now presented. First, the upstream boundary layer is described. The Van Driest velocity is presented Figure 3(a) in wall coordinates and compared with theoretical log law for turbulent boundary layers. The friction velocity u_τ has been evaluated to $22.6ms^{-1}$, which corresponds to a friction coefficient of 2.2×10^{-3}. The displacement thickness is of

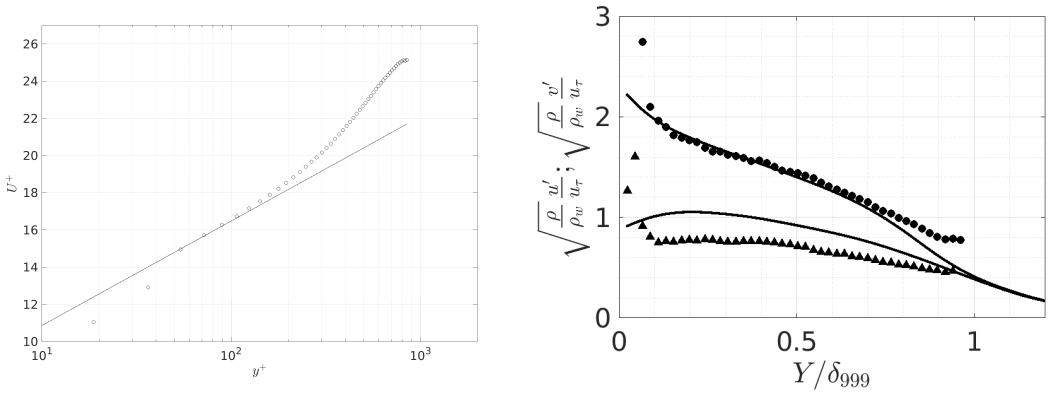

(a) (b)

Fig. 3 Velocity fields upstream from the expansion. (a) mean longitudinal velocity (VanDriest's transform); (b) longitudinal and vertical velocity fluctuations (Morkovin's representation). •longitudinal velocity fluctuations, ▲ vertical velocity fluctuations. Lines correspond to subsonic data [11]

1.7mm. The longitudinal and normal velocity fluctuations are reported Figure 3(b) using Morkovin's representation and compared with incompressible boundary layer results. The upstream flow exhibits classical properties of zero pressure gradient turbulent boundary layers.

Thanks to the static pressure measurements, the spatial organization of the interaction is now characterized. The longitudinal pressure evolution through the interaction at the wall is shown in figure 4(a) for the ($\dot{m}_1$,θ=6.5 °) configuration .

The shape of the pressure gradient through the shock exhibits two steps. The Free Interaction Theory states that, for a separated configuration, the wall pressure rise in the interaction can be expressed as follows: ([12])

$$\frac{P(\bar{x}) - P(\bar{x_0})}{q_0} = F_{fit}(\bar{x}) * \sqrt{(\frac{2 * Cf}{\sqrt{(M_1'^2 - 1)}})} \tag{1}$$

Where:

- x_0 is the interaction's origin, where the adverse pressure gradient initially "influences" the boundary layer.
- l is the distance between x_0 and the separation point x_s.
- q_0 is the dynamic pressure upstream the pressure rise (downstream the expansion in our study).
- F_{fit} is a universal function depending only on the flow regime: $F_{fit}(x_s) = 4$ and in the separated region $F_{fit}(x_{plateau}) = 6$, in a turbulent flow regime.
- Cf is the friction coefficient upstream the pressure rise (downstream the expansion in our study).
- M_1' is the Mach number upstream the pressure rise (downstream the expansion in our configuration).

Therefore, Chapman theory suggests that, for a separated flow, the pressure rise from the interaction's origin until the separated area depends only on the incoming boundary layer properties and it does not depend on the configuration downstream the separation.

We present on the figure 4(a) the normalized pressure quantity $F_{fit}(\bar{x})$ and the theoretical values $F_{fit}(x_s) = 4$ and $F_{fit}(x_{plateau}) = 6$.

Therefore, the wall pressure profile presented Figure 4(a) is coherent with a separated interaction as proposed in the Free Interaction Theory. This point will be validated further from PIV results.

The mean and turbulent longitudinal velocity profiles in the boundary layer downstream the expansion, but upstream the initial pressure rise due to the head shock, are superimposed to the upstream profile on the figure 4. The displacement thickness and Mach number in the downstream boundary layer are respectively 1.75mm and 2.4. The mean velocity profile is clearly distorted compared with the upstream boundary layer showing that the boundary layer has not relaxed from the expansion. Mean and turbulent fields in the interaction have been documented thanks to PIV measurements. PIV results are illustrated in figures 5(a) and 5(c) where the fields of the mean longitudinal velocity and rms vertical velocity along the flow, normalized by the external velocity, are presented. The deviation of the supersonic flow due to

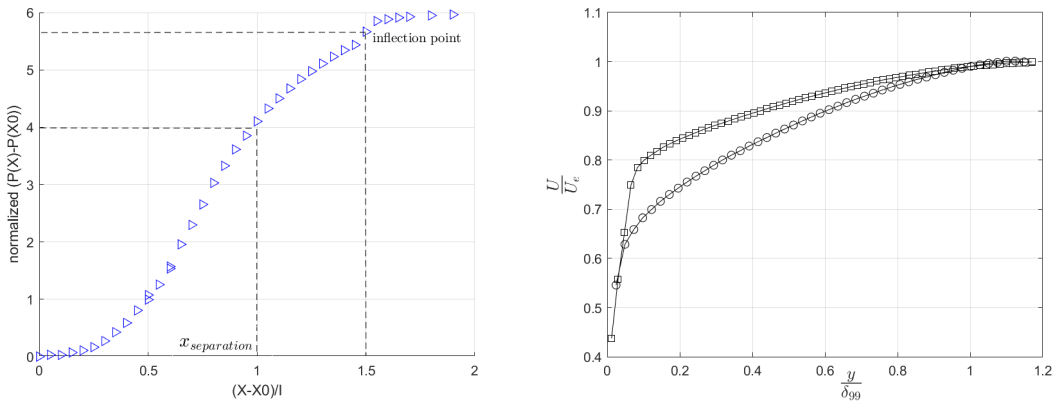

Fig. 4 (a) Expansion and Compression through the interaction at y=9mm from the wall for ($\dot{m} = \dot{m}_1$,θ=6.5 °,$\frac{P_2}{P_1'} = 2.1$) configuration; (b) longitudinal mean velocity ; (c) longitudinal and normal velocity fluctuations; (o : undisturbed boundary layer, □: Boundary layer after expansion).

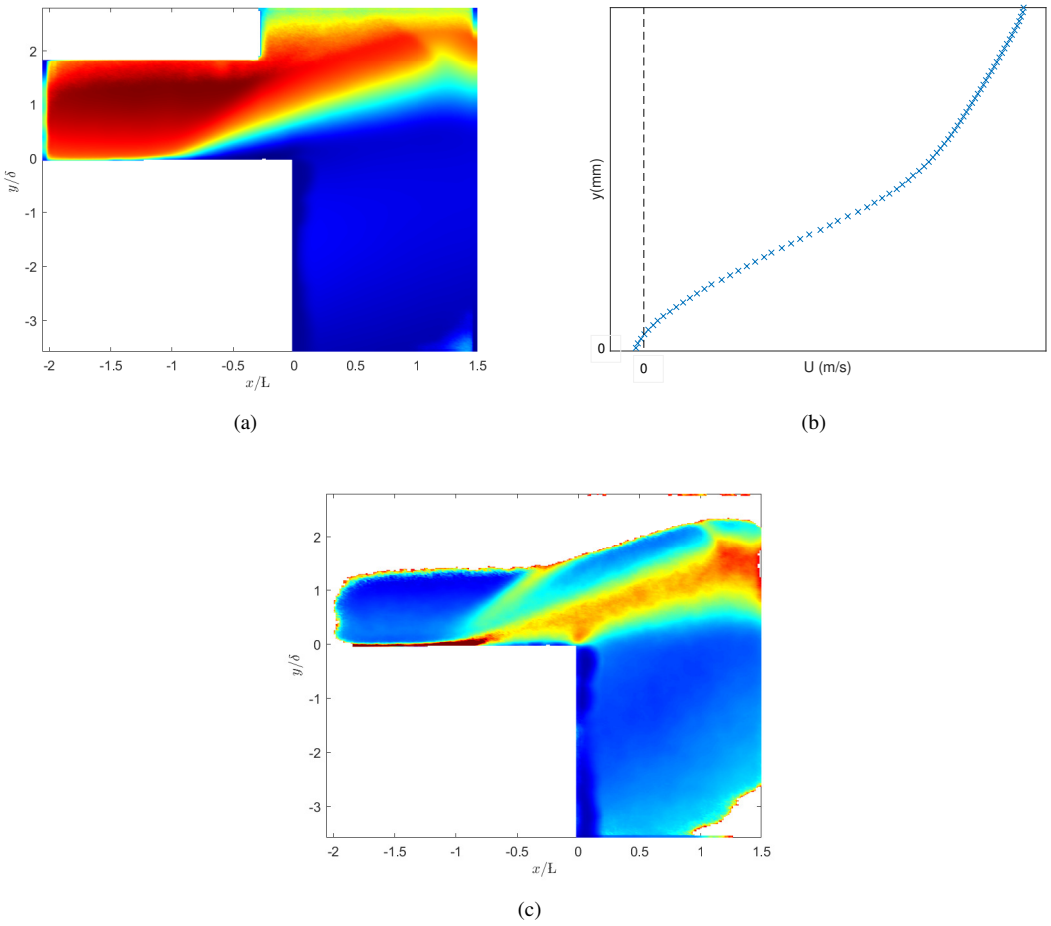

Fig. 5 Velocity fields downstream the expansion for the ($\dot{m} = \dot{m}_1$,θ=6.5 °) configuration. (a) mean longitudinal velocity ; (b) Velocity profile in the separation; (c) Vertical velocity standard deviation

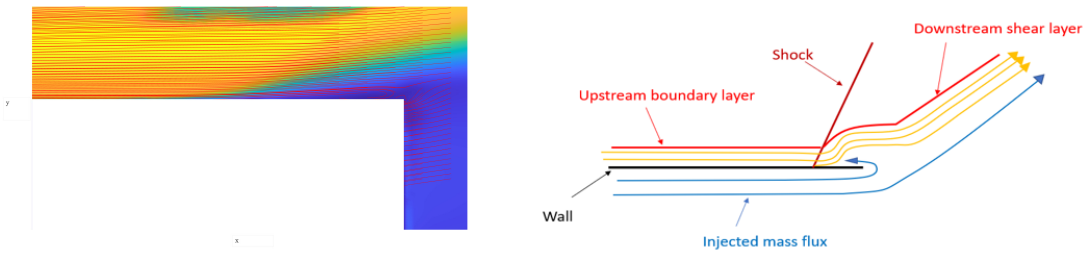

(a) (b)

Fig. 6 (a) Pseudo-streamlines near the separation region for ($\dot{m} = \dot{m}_1$,θ=6.5 °) configuration; (b) Scheme of the present free separation

the over-pressured subsonic injection is clearly seen. A uniform deviation is observed which extends more than one length of interaction downstream from the lip. It is then deviated due to the interaction with the reflected shock of the expansion generator leading edge shock. This confirms that this configuration is similar to a Free Separation. A velocity profile inside the interaction is reported in figure 5(b) to illustrate the flow separation, as it was suggested from the pressure measurements. The separation shock is clearly highlighted from the standard deviation vertical velocity measurement and allows to evaluate the length of the interaction L defined as the distance of the shock foot from the lip where the secondary flow is merging with the supersonic one.

An intense turbulent region is also identified from the vertical velocity fluctuations in vicinity of the lip, which suggests a strongly unsteady behavior in this region, with significant vertical motions. In order to detail the mean flow organization in this region, pseudo-streamlines derived from the mean 2D-2C velocity field are reported figure 6(a). From this figure, it is obvious that the region of high velocity fluctuation intensity near the lip has to be related with the strongly curved streamlines associated with the reverse flow in the separated region. The pseudo-streamlines show that a slight part of the secondary flow is injected inside the recirculating region.

The flow organization is therefore quite similar to a classical separated compression corner configuration, with the difference that a continuous fluid injection is present in the vicinity of the lip, supplying the detached zone. This is illustrated on the scheme shown figure 6(b). This is an important difference when models based on mass conservation are considered. Piponniau's et al. [1] proposed to relate the low frequency unsteadiness observed in separated SWBLI to the unbalanced flow mass in the separated region due to the mass entrainment of the separated shear layer [1]. In our case, such unbalance is unlikely to be expected, which could suggest a low frequency unsteady behavior significantly modified with respect to the classical SWBLI.

Other models for the description of the low frequency unsteadiness in SWBLI were based on the mean flow topology. For example, Touber et al. [4] used the mean flow properties in the initial part of a shock reflection to derive a differential equation suggesting that the interaction could behave as a low pass filter for the upstream perturbations. In our case, the initial part of the interaction is very similar to a classical compression corner flow, and similar results could be derived. Other results, derived from global stability analysis [5], also proposed to relate the unsteady low frequencies in separated SWBLI to an equivalent low pass filter. In these cases, the global mean field, down to the reattachment, is considered. Therefore, it is possible that in this new configuration, where the mean field is significantly modified in the downstream region of the interaction, different results could be derived. It is therefore of interest to describe the time properties of this new type of interaction in order to compare the results with the different models proposed in re-attaching SWBLI. This is done in the next section using simultaneous wall unsteady pressure and hot wire measurements.

V. Characterization of the separation shock unsteadiness

The hot wire anemometry allows to estimate the excursion length L_{exp} of the shock. When the hot wire probe is upstream or downstream from the shock, the signal measured by the hot wire is almost constant (on high or low level) so the rms of the voltage fluctuations σ_e is minimal. However, when the probe is at the mean position of the shock, the signal is fluctuating between the highest and the lowest levels so σ_e is maximal. Results are shown in figure 7.

A gaussian fit applied on the longitudinal evolution of σ_e is shown on the figure. The length of exploration of the separation shock L_{exp} is defined as twice the standard deviation of the curve. We find $\frac{L_{exp}}{L} = 0.15$. Similar evaluations

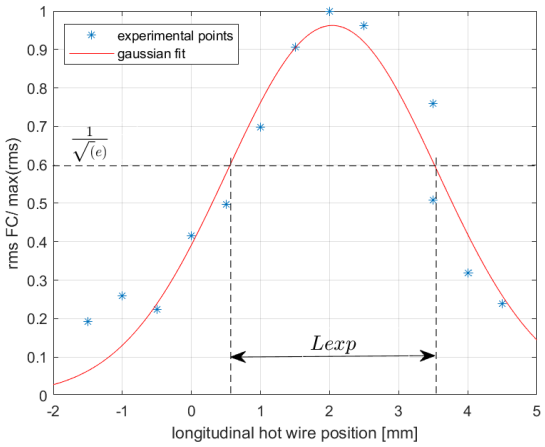

Fig. 7 Longitudinal rms evolution of the hot wire signal along the separated shock for ($\dot{m} = \dot{m}_1$,θ=6.5 °,$\frac{P_2}{P_1'} = 2.1$) at y=15mm. Red line is the best Gaussian fit

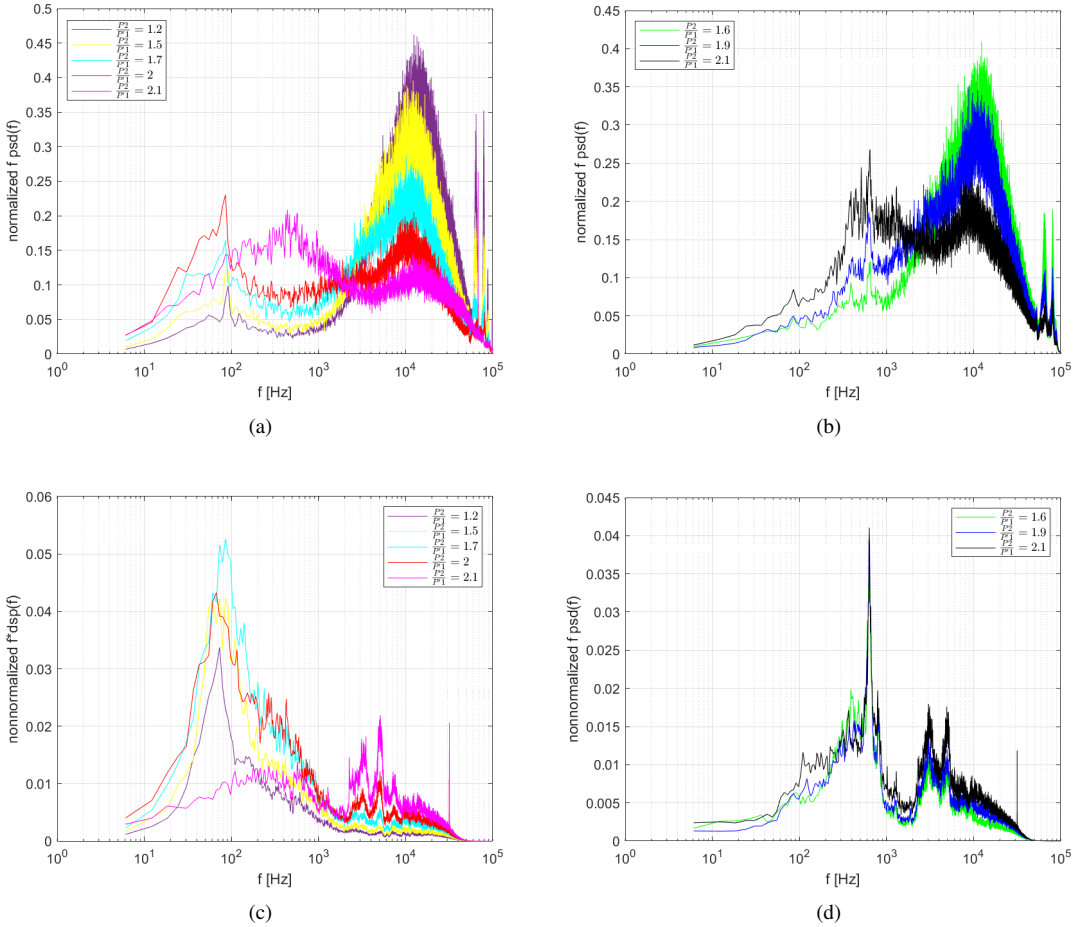

Fig. 8 Pre-multiplied Power Spectral Density for various pressure ratio $\frac{P_2}{P_1'}$; (a)and (b) hot wire signals at the mean shock location respectively at $\dot{m}_1$ et $\dot{m}_2$; (c) and (d) kulites signals at the floor of the secondary flow respectively at $\dot{m}_1$ et $\dot{m}_2$

of L_{exp} have been derived for cases corresponding to pressure ratio ranging from 1.5 to 2.1. The observed lengths of exploration are found similar to those observed in a Mach 2.3 shock reflection at similar Reynolds number [13].
The characteristic time scales of the flow have been evaluated from simultaneous in field hot wire measurements and unsteady pressure sensors (Kulites) placed at the floor of the secondary subsonic flow downstream from the lip and inside the pipes upstream of the exit section of the injection system. The pre-multiplied Power Spectral Density of the hot wire signals recorded at the mean position of the head shock and of the Kulite sensor placed at the floor are reported on Figure 8 for a wide range of pressure ratio $\frac{P_2}{P_1'}$ which covers attached to separated cases. The onset of separation has been found around $\frac{P_2}{P_1'} = 1.9$. These pressure ratios have been obtained with two different secondary mass flow: respectively noted $\dot{m}_1$ and $\dot{m}_2$ and different expansion (from 3 to 6.5 °). Two cases corresponding to a pressure ratio of 2.1 have been obtained using the two different secondary injection: they are reported respectively in black ($\dot{m}_2$ and 6 °expansion) and magenta ($\dot{m}_1$ and 6.5 °expansion) and are referred respectively a P2-6.0 and P1-6.5 cases.
In all cases, high frequency content $f > 10kHz$) can be observed. This range of frequencies has to be related to the time scales of the energetic eddies of the upstream turbulent supersonic boundary layer. Two other range of lower frequencies ($f_1 < 100Hz$ and $100Hz < f_2 < 1kHz$) are also observed. From the incipient case to the separated one, the relative contribution of the low frequencies f_2 to the hot wire signal is increasing. In other words, the energetic content of the shock seems dominated by low frequencies when the separation gets stronger.
Such low frequencies could be compared with the low frequencies observed in classical SWBLI: in these flows, Strouhal numbers defined as $S_L = f_2 L/U_1$ where U_1 is the velocity downstream the separated shock, where found around 0.03. In our case a value of 0.02 is obtained, which is quite similar. The two cases P2-6.0 and P1-6.5 exhibit different spectra in the low frequency domain: this point is developed further.
As previously mentioned, these cases are involving two different secondary subsonic flows. In order to qualify the temporal properties of these two cases, the PSD derived from the kulite signals are reported for the sames configurations as the shock signals on Figure 8 . Two families of PSD are clearly obtained. The first one corresponds to the cases $\frac{P_2}{P_1'}$ =1.5, 1.7 and 2 when the second one corresponds to the cases $\frac{P_2}{P_1'}$ =1.6, 1.9 and 2.1, case P2-6.0. The firsts correspond to a $\dot{m}_1$ secondary flow when the other are associated with a $\dot{m}_2$ secondary flow. In this case, a characteristic frequency of 6kHz is clearly visible and is associated with some acoustic resonance in the injection pipes, as it was controlled from the Kulite sensor placed in these pipes. Such resonance is not visible for the P1-6.5 case.
When the shock signal are considered, it is clear that they involve similar frequencies to that of the unsteady pressure signals which are recorded at the wall, under the subsonic flow. For example, the acoustic frequency observed with the $\dot{m}_2$ secondary flow is also clearly found in the corresponding shock PSD. The P1-6.5 case is an intermediate case: no acoustic perturbations is observed from the secondary flow, but the shock as well as the wall pressure signals differ from the other $\dot{m}_1$ cases. In summary, whatever the state of separation and the nature of the secondary flow, the shock signals and the wall pressure signals involve quite similar time scales, suggesting a strong links between both signals. This is illustrated on Figure 9 where the coherence function between the hot wire and Kulite signals are reported for the same cases as Figure 8. The two different secondary flows ($\dot{m}_1$ and $\dot{m}_2$) are respectively shown on figure 9(a) and figure 9(b). For both cases, a strong coherence between both signals is observed for the most energetic frequencies of the secondary flow (see figure 8).
In order to evaluate the link between the unsteadiness of the shock and the flow downstream the interaction, we define a transfer function $H(f)$ that is the ratio between the PSD of the shock motions and the flow downstream spectrum. $H(f)$ has been evaluated for the different cases of pressure ratio and is reported on figure 10(a). From the figure, it is clear that, as the intensity of the interaction increases, the relative proportion of the high frequencies in the shock motions (associated to the upstream perturbations, O(10kHz) to the lower frequencies present in the secondary flow (f<1kHz) is decreasing. The hot wire signals are not able to describe directly the shock motions, but only the time history of its passage upstream and downstream from its mean position. Therefore, the increasing relative energy of the low frequencies suggests that the amplitude of the motions of the shock involving these low frequencies is also increasing, relatively to those associated with the high frequencies. That suggests that the low frequency motions of the shock are probably due to the secondary flow unsteady conditions, but that its amplitude response depends on the intensity of the interaction, with a maxima when the flow separates.
To complete this first overview of the time organisation of the shock motions, the phase relationships derived from simultaneous kulite and hot wire anemometry are shown Figure 10(b). For all cases, the phase tends to 0 for the lowest frequencies, which shows that upstream motion of the shock (leading to an increase of the hot wire signal) corresponds to an increase of the downstream pressure. This is a different behavior than observed in classical SWBLI, where an out of phase relationship was observed between the shock motions and the pressure signals at the reattachment point

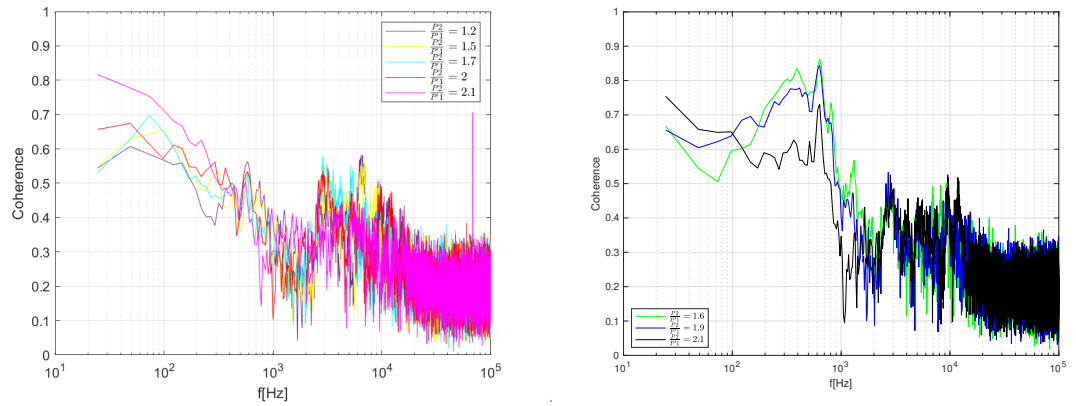

Fig. 9 Coherence between hot wire signals and Kulite sensors for various pressure ratio $\frac{P_2}{P_1'}$; (a) secondary flow at $\dot{m}_1$; (b) secondary flow at $\dot{m}_2$

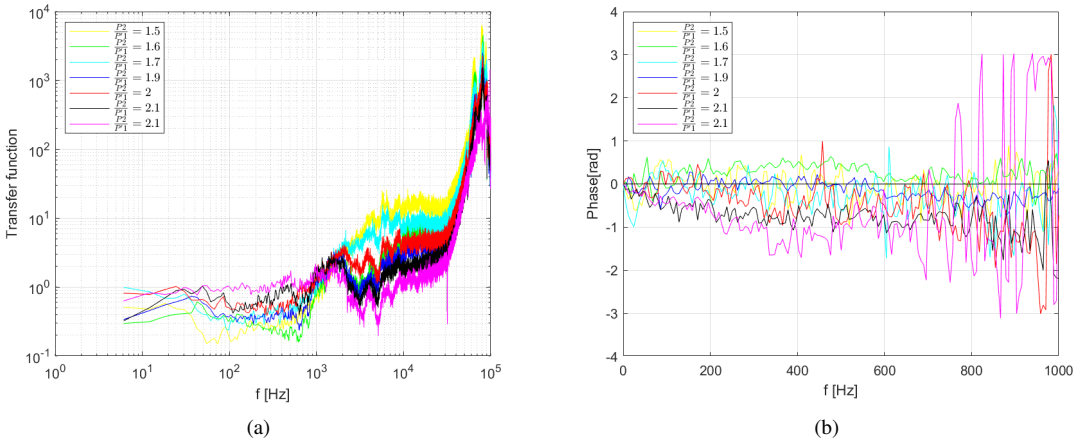

Fig. 10 (a)Transfer function between the shock and the flow downstream unsteadiness; (b) Phase between the shock signal and the flow downstream pressure unsteadiness

[13, 14]. As for the transfer function, a clear tendency, from the attached to the separated cases, can be observed. For the attached cases, the signals are nearly in phase, when a negative phase is observed for the separated cases. This indicates that, from the Fourier analysis, a direction of propagation from the secondary flow to the shock signal can be observed. The different results derived from the PSD, the transfer function and the phase relationships show that the low frequency unsteadiness in the present configuration differ significantly with those observed in classical SWBLI, such as shock reflection or compression corner. They seem to depend strongly on the downstream conditions, with an influence of the separation state on the associated amplitudes of the shock motions.

VI. Conclusion

This study gives an overview of a new 2D SWBLI setup similar to a Free Shock Separation configuration obtained in overexpanded nozzles. The main difference with classical SWBLI as compression corner and shock reflection is that the shear layer issued from the separation point does not reattach downstream and that some mass flux can be injected in the recirculating region. The main space and time scales of the flow have been documented for a wide range of configurations, corresponding to attached as well as separated cases and for two different secondary flow. Evidences of

flow separation have been given with some injection of the secondary flow inside the separated region. When time scales of the shock separation are considered, no evidence of intrinsic low frequencies time scales has been observed and the PSD of hot wire signals recorded at the mean position of the shock are found similar to the PSD of the wall unsteady pressure measured in the secondary subsonic flow. Over-imposed are high frequencies motions, which are probably to be related to the high frequency unsteadiness of the upstream turbulent boundary layer.
Nevertheless, it seems that the low frequency motions of the shock are more important when the flow is separated, suggesting that the interaction reacts differently in amplitude to downstream perturbations when the flow is separating. These findings suggest that the origin of the low frequencies in classical re-attaching SWBLI has to be related with their specific flow topology near the reattachment, as already suggested in various models.

Acknowledgments

The project leading to this publication has received funding from the CNES through the research program ATAC as well as from Excellence Initiative of Aix-Marseille University-A*MIDEX, a French "Investissements d'Avenir" programme. It has been carried out in the framework of the Labex MEC. These supports are gratefully acknowledged.

References

[1] Piponniau, S., Dussauge, J. P., Debiève, J. F., and Dupont, P., "A simple model for low-frequency unsteadiness in shock-induced separation," *Journal of Fluid Mechanics*, Vol. 629, 2009, pp. 87–108.

[2] Plotkin, K., "Shock wave oscillation driven by turbulent boundary layer fluctuations," *AIAA Journal*, Vol. 13, No. 8, 1975, pp. 1036–1040.

[3] Poggie, J., and Smits, A., "Experimental evidence for Plotkin model of shock unsteadiness in separated flow," *Physics of Fluids*, Vol. 17, 2005, pp. 018107.1–18107.4.

[4] Touber, E., and Sandham, N., "Low-order stochastic modelling of low-frequency motions in reflected shock-wave/boundary-layer interactions," *Journal of Fluid Mechanics*, Vol. 671, No. 3, 2011, pp. 417–465.

[5] Sartor, F., Mettot, C., Bur, R., and Sipp, D., "Unsteadiness in transonic shock-wave/boundary-layer interactions: experimental investigation and global stability analysis," *Journal of Fluid Mechanics*, Vol. 781, 2015, pp. 550–577. https://doi.org/10.1017/jfm.2015.510, URL https://www.cambridge.org/core/article/div-class-title-unsteadiness-in-transonic-shock-wave-boundary-layer-interactions-experimental-investigation-and-global-stability-analysis-div/F132D0825352C6EEC1236C9DC24EE445.

[6] Bonne, N., Brion, V., Garnier, E., Bur, R., Molton, P., Sipp, D., and Jacquin, L., "Analysis of the two-dimensional dynamics of a Mach 1.6 shock wave/transitional boundary layer interaction using a RANS based resolvent approach," *Journal of Fluid Mechanics*, Vol. 862, 2019, pp. 1166–1202. https://doi.org/10.1017/jfm.2018.932, URL https://hal.archives-ouvertes.fr/hal-02906114.

[7] Ganapathisubramani, B., Clemens, N. T., and Dolling, D. S., "Effects of upstream boundary layer on the unsteadiness of shock–induced separation," *Journal of Fluid Mechanics*, Vol. 585, 2007, pp. 369–394.

[8] Priebe, S., Tu, J. H., Rowley, C. W., and Martín, M. P., "Low-frequency dynamics in a shock-induced separated flow," *Journal of Fluid Mechanics*, Vol. 807, 2016, pp. 441–477. https://doi.org/10.1017/jfm.2016.557, URL https://www.cambridge.org/core/article/div-class-title-low-frequency-dynamics-in-a-shock-induced-separated-flow-div/105342B205DC3D4581DD5AA262E9A9FE.

[9] Chapman, D. R., Kuehn, D. M., and Larson, H. K., "Investigation of separated flow in supersonic and subsonic streams with emphasis of the effect of transition," Tech. rep., 1957.

[10] Souverein, L., Bakker, P., and Dupont, P., "A scaling analysis for turbulent shock wave boundary layer interactions," *Journal of Fluid Mechanics*, Vol. 714, 2013, pp. 505–535. https://doi.org/10.1017/jfm.2012.495.

[11] Klebanoff, P., "Characteristics of turbulence in a boundary layer with zero pressure gradient," Tech. rep., NASA, 1955.

[12] Chapman, R., and Kuehn, D., *Preliminary report on a study of separated flows*, NACA RESEARCH MEMORANDUM, 1956.

[13] Dupont, P., Haddad, C., and Debiève, J. F., "Space and time organization in a shock induced boundary layer," *Journal of Fluid Mechanics*, Vol. 559, 2006, pp. 255–277.

[14] Debiève, J. F., and Dupont, P., "Dependence between shock and separation bubble in a shock wave / boundary layer interaction," *Schock Waves*, Vol. 19, No. 6, 2009, pp. 499–506.